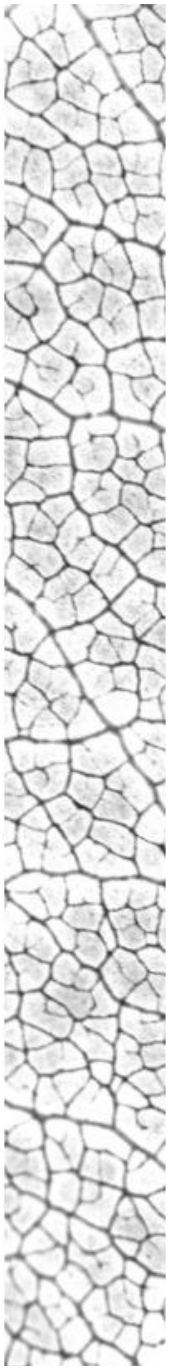

EurAsian Journal of BioSciences
Eurasia J Biosci 14, 219-225 (2020)

Biomechanics of the deformity of septal l-struts

P. V. Pimanchev [1*], I. V. Reshetov [1], D. A. Sidorenkov [1], N. C. Sukortseva [1], K. B. Lipsky [1], G. A. Aganesov [1], Yu. P. Zezin [1], P. V. Chistyakov [1]

[1] State Budgetary Educational Institution of Higher Vocational Education – The First Moscow State Medical University named after I.M. Sechenov, RUSSIA
*Corresponding author: P. V. Pimanchev

Abstract

Objectives/Hypothesis. During septoplasty, an L-shaped septal strut is often preserved or created. The main goal here is to straighten the nasal septum and to provide the required stiffness of the same. Insufficient stiffness of the septum leads to exceeding the maximum permissible value of its deformation and or its excessive deviation, that could result in functional or aesthetic complications. The aim of this work is to study the influence of the geometrical shape of an L-shaped strut on its stiffness. **Designed and testing tools.** With the use of means of computer simulation, we developed L-strut cartilage models featuring an improved stiffness and resistance to deformation. On this basis, we developed L-strut models of various shapes from a material simulating the mechanical properties of cartilage tissue. All the models were tested under the same conditions using a multipurpose instrument ZWICK Z100 and a special device simulating the septum loading conditions. **Methods.** At the first stage of the study, a five-sided septum model was created based on computed tomography scans of human subjects. Then, based on this model, we developed a series of models with various combinations of L-struts, with or without the use of arcs of cartilage. It was assumed that the edges of the septum, connected with the bone support, are fixed, whereas the nasal tip is relatively free-supported. L-strut models were tested under the same loading conditions using a multipurpose instrument ZWICK Z100 and a special device simulating the septum loading conditions. The loading of the models was effected by applying a distributed load along the outer contour, that is the same for all the studied models. On the basis of an experimental data analysis, we assessed the stiffness of the modeled septa. **Results.** We obtained experimental “Force – Travel” dependence for nasal septum models with different geometry. Is shown that a septum with a wider dorsal strut is characterized by the greatest stiffness. **Conclusions.** It is found that a septum with a wider dorsal strut is characterized by the greatest stiffness and a higher resistance to deformation. The preservation of an arc of cartilage and a wider dorsal strut increase the overall stability of the structure.

Keywords: nasal septum, septal l-strut, septal deviation, stiffness, physical modeling, experiments

Pimanchev PV, Reshetov IV, Sidorenkov DA, Sukortseva NC, Lipsky KB, Aganesov GA, Zezin YuP, Lokoshchenko AM (2020) Biomechanics of the deformity of septal l-struts. Eurasia J Biosci 14: 219-225.

INTRODUCTION

During septoplasty, a septal L-strut is often preserved or created, having the form of an L-shaped cartilage spacer element in the nasal dorsal and caudal areas. The main objective here is to ensure the structural stability and to strengthen the nasal septum. Deformation or excessive deviation of such L-strut may cause functional or aesthetic complications, such as twisted nose, malpositioned nasal tip, saddle deformity, and nasal valve insufficiency (Kim and Gurney 2006). Deformations, such as deviation or buckling of the septal L-strut, represent a mechanical and structural problem. Nevertheless, there is a relatively small number of studies available that investigate various factors, such as the design of a septal L-strut and the loads affecting its stability. Mau et al. (2007) described a simplified L-strut model that was built on the basis of a (four-sided) rectangular model of the nasal septum. This study included a digital simulation of the influence of various configuration on the L-strut stability. Based on the data of finite element analysis, it was demonstrated that the intrinsic elasticity of the septal cartilage, the mucoperichondrial flap and the overlap with the bony vault all contributed to the required stiffness and stability of the L-strut (under normal conditions). However, in case of an accident overload, this level of stiffness can lead to the development of unacceptable septum deformation values. Enhancing the stiffness and stability

Received: January 2019
Accepted: November 2019
Printed: March 2020

of the entire structure (nose) can be achieved by preserving a small cartilage segment in the bony-cartilaginous (BC) junction of the dorsal L-strut. However, this model is simplified, as its authors proceed from the fact that all the cartilaginous supporting edges of the nasal septum were free edges, which was not representative of the actual boundary conditions in the nasal septum (Salalykina and Papikyan 2018, Ilchenko et al. 2018).

According to Westreich and Lawson (2008), the combined medial crura and the lower lateral cartilages (LLCs) form a tripod that rests on the anterior nasal spine. Furthermore, the nasal tip exhibits elastic behavior due to the LLCs, which produce an upward force in the form of stored elastic potential energy. Therefore, the nasal tip is not a completely free element. Another significant limitation in the work by Mau et al. (2007) is the exclusion of the portion of the septal cartilages connected to the nasal bone.

In the work of Lee et al. (2010), the initial rectangular model of the nasal septum, as suggested by Mau et al. (2007), was replaced with a five-sided model, that reflects more accurately the shape of a real nasal septum.

Besides, the obtained simulation models were added with a nasal septum support. The authors concluded that a spring-supported nasal tip model gives a more accurate representation of the boundary junctions inside the nose. It was found that both in free-supported and spring supported nasal tip, the BC junction and the nasal spine are the main points of maximum stress regardless of material properties. The preservation of an arc of cartilage and a wider dorsal strut increase the stability of the structure.

For further development of model representations by Mau et al. (2007) and Lee et al. (2010) about the nasal septum structure, in this paper the initial four-sided and five-sided simulating models were replaced with a new five-sided model of an L-shaped strut made of a synthetic material, that is similar, in terms of its properties, to the septal cartilage tissue.

The new model additionally includes an arc of cartilage in the inner corner of the L-strut, and fixed caudal and dorsal ends of this structure, because in reality these areas are connected with the nasal spine of the upper jaw in the caudal area and with nasal bones in the dorsal area.

MATERIALS AND METHODS

Generation of the Computed Tomography Scan

Cranial computed tomography (CT) scans were taken from a specific patient with an undeviated nasal septum. The patient was chosen because he had neither previously undergone septoplasty or rhinoplasty nor was subjected to injury to the nose. In the CT scan, x-ray images were taken of the head, one narrow slice at a time (Harris 2010).

Using the certified software Mimics (Materialise Technologies, Leuven, Belgium), by the method of superposition of the x-ray images, a three-dimensional model was created reflecting the nasal septum attachment area of the patient under examination.

Geometry of the CT Scan and Studied Nasal Septum Models

Fig. 1 shows the photos of nasal septum models under study. The models are built based on the computed tomography, various anatomical features and includes the bony-cartilaginous junction, where the nasal bone and the dorsal nasal spine are connected. L-strut models were generated after exclusion of the rectangular element of cartilage (**Fig. 1B**). To investigate the influence of including an arc of cartilage on the stress occurring in the model, another model was built based on CT scans (**Fig. 1C**).

As recommended (Mau et al. 2007), all the models were characterized by a strut with a 16 mm dorsal section. One model was built with no arc of cartilage (Model A), the second one, with an arc of cartilage in the inner corner (Model B), the third one, with an arc of cartilage in the dorsal section (Model C), and the forth one, with two arcs of cartilage both in the dorsal area and in the inner corner (Model D). The thickness of the models was selected according to data of Mau et al. (2007) and Lee at al. (2010) and was equal to 2 mm.

Material Properties

Cartilage, like other living tissues, has a non-homogenous, anisotropic, nonlinear, viscoelastic behavior, and its properties depend on the history of applied loads (Vicente et al. 2008). However, in this study, to investigate the influence of the septal strut shape on the nasal septum stiffness, it was adequate to model the cartilage as a homogenous elastic material with similar mechanical characteristics. Deformations below 20% (Vicente et al. 2008) lead to significant changes in cartilage, and such an approach to modeling is sufficiently reasonable [6]. In addition, it allowed us to simplify the comparison of the physical modeling results with the data presented in Mau et al. (2007) and Lee et al. (2010), because these authors also proceeded from the assumption of the nasal septum linear elasticity.

Tensile Elastic Modulus

As reported in the papers of Grellmann et al. (2006) and Richmon et al. (2005), the range of the tensile modulus ranged from 2.62 MPa to 10.6 MPa. Such a wide variation of values is due to the difference in collagen fibril arrangement from one person to another. The collagen fibrils within cartilages determine its tensile behavior.

For small deformations in tension, when the tensile stress in the cartilage is small, a nonlinear toe region is seen in the stress-strain curve, due to realignment of the

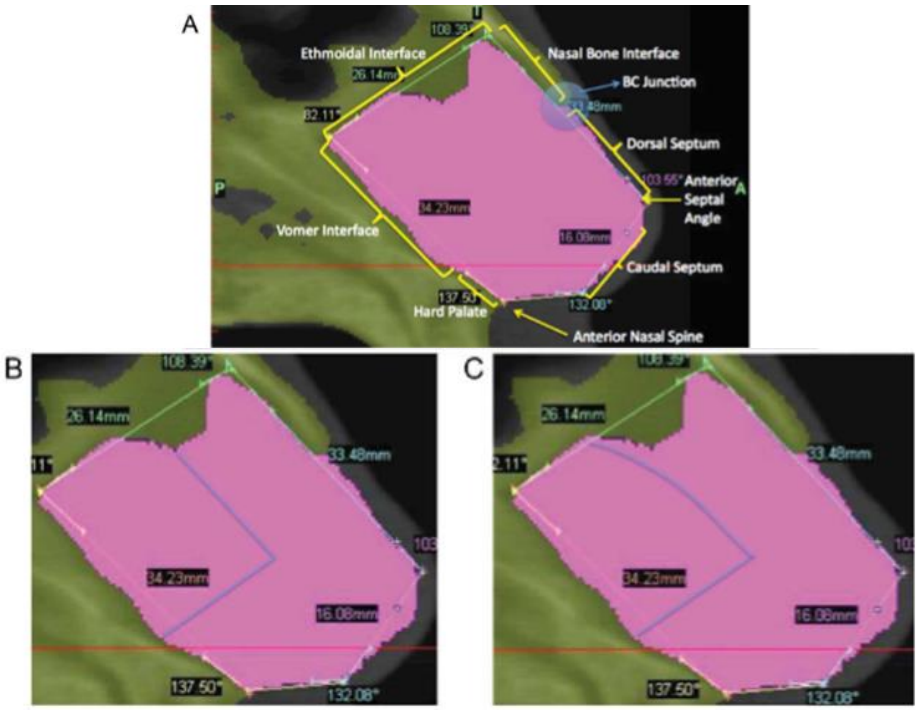

Fig. 1. Computed tomography (CT) scan of the nasal septum. (A) CT scan with indicated anatomical features. (B) CT scan with outlined L-strut model. (C) CT scan with outlined L-strut model including an arc of cartilage

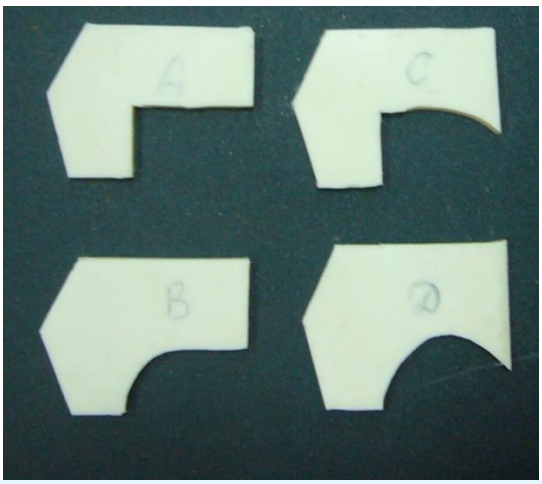

Fig. 2. Finite element models. Model A with no arc of cartilage; Model B with an arc of cartilage in the inner corner; Model C with an arc of cartilage in the dorsal section; Model D with two arcs of cartilage both in the dorsal section and in the inner corner

collagen fibrils. However, for larger deformations, after realignment, collagen fibrils are stretched and therefore generate a larger tensile stress due to the stiffness of the collagen fibrils (Wilson et al. 2005). Therefore, the tensile stiffness of cartilage is highly dependent on strain.

Compressive Elastic Modulus

According to Richmon et al. (2006) and the measurement the nasal septum in the vertical, caudal-cephalic, and the medial directions, the range of the compressive modulus ranged from 0.40 MPa to 0.83 MPa. Such a wide range of values is due to the presence of interstitial fluid between the collagen fiber and proteoglycan (PG) network. Under a compressive load, the aggrecan molecules, which are attached to the PG network, are pushed closer together [11]. This causes greater repulsion between the PG side chains. To balance this increase, more water is drawn in, thus increasing osmotic pressure. Therefore, the compressive stiffness increases with decreasing volume (2005). Furthermore, a different network of molecules implies different compressive behavior.

Poisson's Ratio

According to Grellmann et al., the Poisson's ratio was found to range from 0.26 to 0.38. According to Garcia [12], the inconsistency is due to the constraints in the grips, the stress field under a tension test being really two-dimensional, and Poisson's ratio depends on the aspect ratio of the specimen used in the experimental set-up.

Model Material Properties

The material used in this study to simulate the nasal cartilage properties was polydimethylsiloxane reinforced by silicon dioxide nanoparticles ("Aerosil") with a particle size of 5–40 nm. The filler content in the material was approximately 15% by weight. Adding filler nanoparticles to the composition of the material increased the strength and Young's modulus of the elastomer, while preserving its high elasticity. **Fig. 3** shows a strain diagram of the model material.

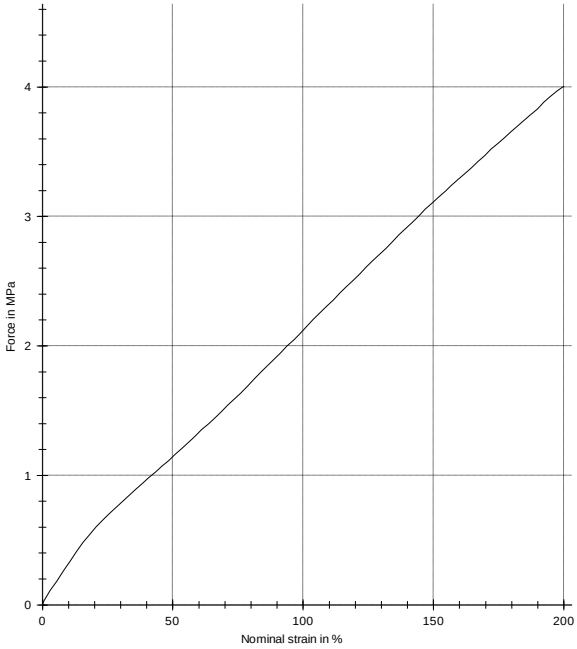

Fig. 3. Strain diagram of filled polydimethylsiloxane, which is generally used for simulating the nasal septum cartilage properties

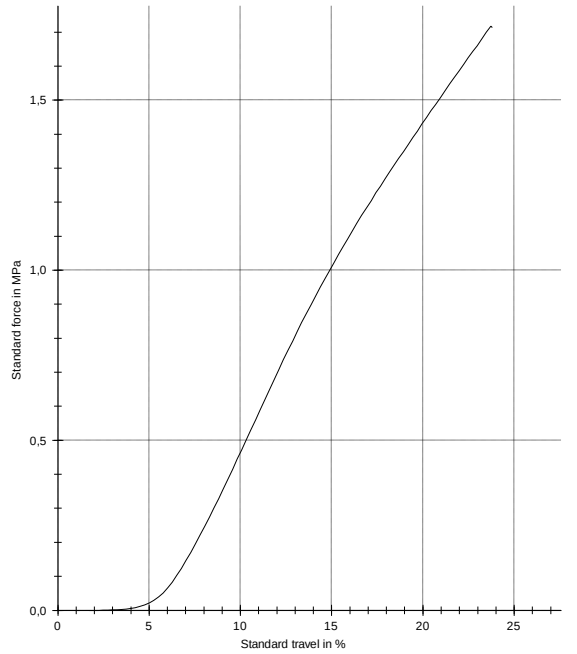

Fig. 4. Strain diagram of filled polydimethylsiloxane, which is generally used for modelling the nasal septum cartilage properties

It should be noted some nonlinearity in the dependence of the stress from the deformation in the initial section of the diagram, which is characteristic of cartilage tissue [5]. The tensile modulus for the model material is 2.5 MPa, which corresponds to the lower end of the range of Young's modulus experimental values for cartilage tissue.

Fig. 4 shows the dependence of stress from the deformation of the model material during compression.

As in the case of tension, we can note some nonlinearity in the compression diagram within the deformation values range of 10–20%. The modulus of compression is about 1 MPa, which corresponds to the upper end of the range of experimental compression modulus values for the nasal cartilage tissue. It should be noted that the selected model material exhibits different values of tensile and compression moduli, that are typical for living tissue of the nasal septum.

Boundary Conditions of the Nasal Septum and Bone Tissue Junction

As shown in **Fig. 1A**, as the junctions of the bone tissue with the nasal septum (ethmoid bone, vomer, hard palate and nasal bone junctions) have a much greater hardness than the septal cartilage itself, it seems logical to assume that these junctions are rigidly fixed (Pena et al. 2007).

Nasal Tip Loading Conditions

For the purpose of this study, the anterior septal angle was assumed to be the nasal tip. In reality, the nasal tip lies anterior to the anterior septal angle, where the lower lateral cartilages meet. However, the assumption is adequate as the distance from the anterior septal angle is small.

According to the tripod theory proposed by Adamson and Funk (Adamson and Funk 2009), the medial crura and paired LLCs form a tripod. However, this theory is only applicable in patients where all three legs of the tripod are equally strong and well supported, which is only seen in a small group of patients. In other cases, when one leg's stability is greater than the others, the most stable leg's fixation point is predominant (Westreich and Lawson 2008). Furthermore, according to Westreich and Lawson (2008), the nasal tip exhibits elastic behavior. This is due to the LLCs, which produce an upward force in the form of stored elastic potential energy (Westreich and Lawson 2008). This, coupled with the unequal stability in the tripod, implies that the LLCs, also referred to as nasal tip cartilages, can be thought of as a spring and a cantilever as they exhibit deformation, recoil, and elasticity (Westreich et al. 2007). In our experiment, we proceeded from the assumption that the nasal tip is in a relatively free position, whereas the dorsal and caudal ends are rigidly supported (**Fig. 5**).

Model Stiffness Tests

For the full-scale experiment, a special device was developed for loading the studied models of L-struts and for assessing their stiffness. **Fig. 5** is a photograph of the used device. In this picture, 1 is the L-strut model with arcs of cartilage in the inner corner and in the dorsal segment. The model is mounted on a support member

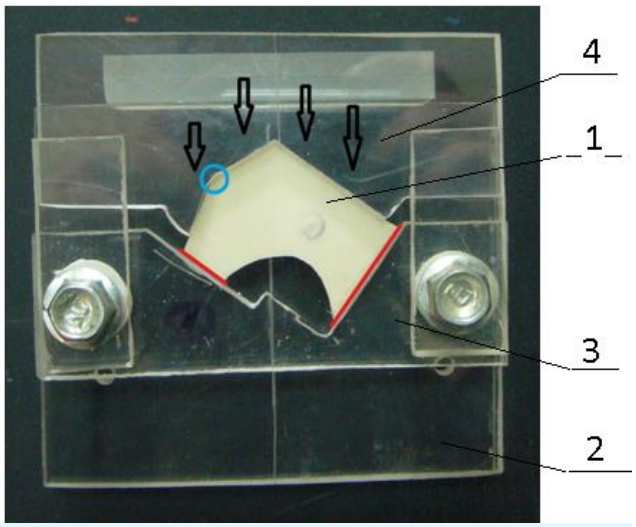

Fig. 5. Device for full-scale tests of nasal septum models. 1 – L-strut model with preservation of arcs of cartilage in the inner corner and in the dorsal segment. 2, 3, 4 – elements for the device for full-scale tests. The nasal tip is the section marked by a small blue circle. The red lines indicate the model areas that correspond to bone tissue and nasal septum junctions – those with the ethmoid bone, the vomer, the hard palate, the nasal bone and the nasal spine of the upper jaw. The black arrows indicate the model loading directions

Fig. 6. Device for measuring the stiffness of nasal septum models in the grip of the ZWICK Z100 instrument

3, that is rigidly connected to the device base 2. A base 2 is mounted in a fixed grip of the material testing instrument ZWICK Z100. The model loading is performed through a loading element 4, the movement of which, with a constant velocity, is initiated through a mobile grip of the device. The nasal tip is the area marked in the photo by a small blue circle. The red lines indicate the areas of the model that corresponds to the junctions of the bone tissue with the nasal septum – the

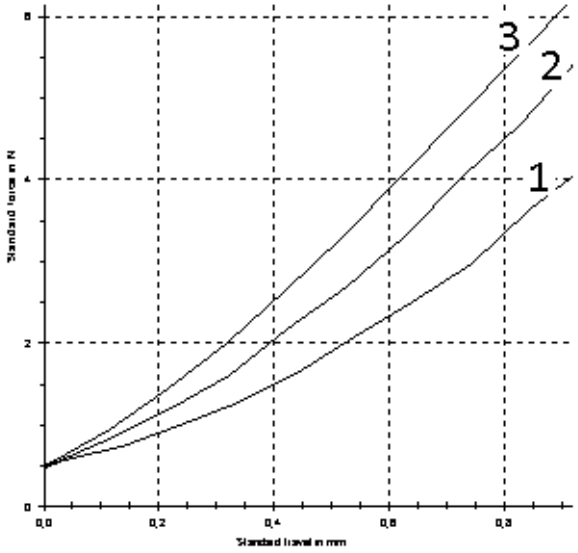

Fig. 7. "Force – Travel" diagrams for the different types of the studied models: 1 – model type B; 2 – model type C, 3 – model type D

Table 1. Summary results of stiffness measures for models B, C, D

Model	Greatest value of the force for the loading element travel of 1 mm (N)	Model stiffness (10^3 N/m)
B	5.4	6.44
C	4	5.04
D	6.2	7.27

junctions with the ethmoid bone, the vomer, the hard palate, the nasal bone and the nasal spine of the upper jaw. The arrows indicate the distributed load on the studies model of the nasal septum.

Fig. 6 is a photograph of the device with the studied model mounted in the grips of the ZWICK Z100 instrument.

The models were tested under the conditions of the constant travel speed of the loading element. The maximum travel was 1 mm. During the tests, we recorded the dependence of the force that was applied to the loading element from its travel amount, which corresponds to the displacement of the the outer contour of the studied model.

RESULTS

The full-scale testing results of studied nasal septum models were obtained in the form of a "Force – Travel" diagrams for the considered type of models. **Fig. 7** shows the detailed diagrams for the B, C and D model types.

The actual stiffness of the studied septa may be measured as the tangent of the inclination angle of the experimental "Force – Travel" diagram at the initial stage of deformation.

The experimental evaluation of stiffness for the studied septa is shown in **Table 1**.

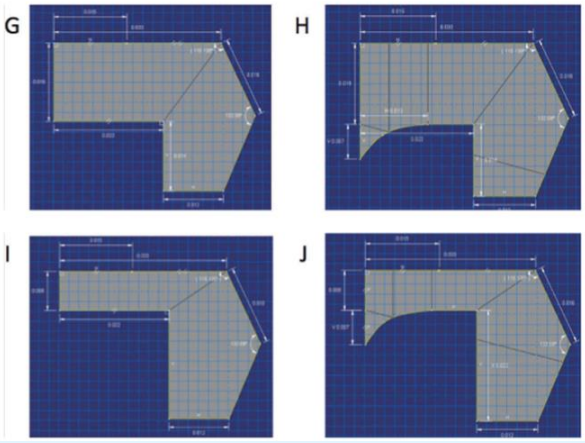

Fig. 8. Finite elements of the nasal septum. Model G with a wider dorsal segment. Model H with a wider dorsal strut, additionally including an arc of cartilage. Model I with a narrower dorsal strut. Model J with a narrow dorsal strut, additionally including an arc of cartilage. The picture is reproduced from the work of Lee et al. (2010)

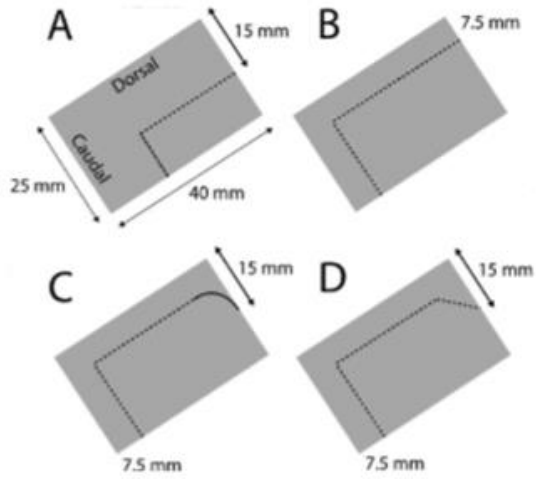

Fig. 9. Mau's L-strut designs. (A) Conventional 15-mm strut. (B) Conventional 7.5-mm strut. (C) Modified 7.5-mm strut with preservation of an arc of cartilage to maintain the 15 mm contact width at the bony-cartilaginous (BC) junction. (D) Modified 7.5-mm strut with preservation of a triangle of cartilage to maintain the 15-mm contact width at the BC junction. Reproduced from Mau et al. (2007)

ANALYSIS OF THE RESULTS

The analysis in the work of Mau et al.[2] was carried out based on the estimated boundary conditions for a free nasal tip. In Lee et al.[16], the analysis was based on the estimated boundary conditions for free and fixed nasal tips. The used simulating models are shown in **Figs. 8** and **9**. The junctions with the ethmoid bone and the hard palate are simulated as rigidly fixed ends. All other areas are simulated as free ends. A common lateral load of 1 N was applied to all models.

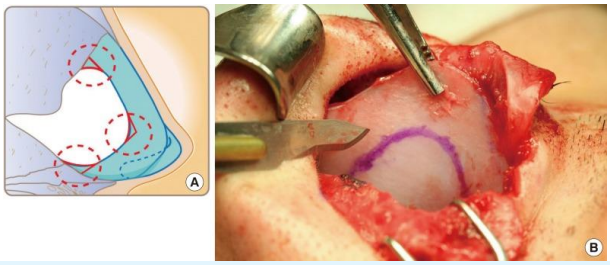

Fig. 10. Creating an L-strut, we should preserve the arcs of cartilage, especially in the inner corner. This enhances the structural stiffness and, therefore, reduces the risks of complications related to the loss of the bearing capacity of an L-shaped strut

In both classes of models – with a free nasal tip and with a spring-supported nasal tip – the BC junction and the nasal spine are the points of maximum stress in the nasal septum. Preserving an arc of cartilage and increasing the dorsal strut length improves the septum stiffness and resistance to deformation.

According to the recommendations of Mau et al. (2007) and Lee and al. (2010), we used in this study a L-strut with a 16 mm wide dorsal segment. We additionally analyzed two new configurations of the nasal septum, one having an additional arc of cartilage in the inner corner (Model B); the second one, with two additional arcs of cartilage: one in the inner corner, and the second in the dorsal segment (Model D). Inclusion of these models was related to our clinical observations. If, during septoplasty, we preserved an arc of cartilage in the inner corner, we obtained a more stable nasal septum than in the absence of such arc of cartilage. As a result, our observations proved to be correct, because B and D L-strut models exhibited a higher stiffness during the tests. The most rigid model was Model D with two arcs of cartilage – one in the inner corner, and the second one, in the dorsal segment.

A traditional guideline for the septal L-strut is to preserve a 1-cm width of L-strut that ensures its structural stability. The present results do confirm this recommendation, as the stress would be higher for the smaller width of L-strut, and more importantly, the stress would be higher for the septum with weaker mechanical strength. Therefore, it is always prudent to preserve as wide as possible the septal L-strut. The arc is also found to reduce the stress level in the septal L-strut (**Fig. 10**) Therefore, further preservation of additional material, especially at the ethmoid region, increases stability. This might be important in a trauma case where there is an associated fracture in the septal cartilage such as "S" and "C" shapes due to intrinsic cartilage fracture.

Limitations

A limitation of the present analysis is the assumption of uniform cartilage thickness. Septal thickness ranges from the thickest along the septal base, followed by the dorsum, central portion, and the anterior septal angle (Mowlavi et al. 2006).

CONCLUSION

This study describes the effects achieved due to the use of L-struts of various configurations. An experimental study of the model stiffness gives clearer results, as compared with simulation studies. The BC junction, the nasal tip and the nasal spine are the points of the maximum stress. Preservation of an arc of cartilage, especially in the inner corner, and a wider dorsal strut enhances the structure stiffness and overall resistance to deformation, as compared with an L-strut with a direct angle.

ACKNOWLEDGEMENT

This work was supported by the Russian Foundation for Basic Research (RFBR) grant № 15-29-04819 “Hybrid structures made of artificial materials created using 3Dprinting with the inclusion of mesenchymal stem cells for the reconstruction of cartilage tissue”.

REFERENCES

Adamson PA, Funk E (2009) Nasal tip dynamics. Facial Plast Surg Clin North Am 17: 29–40.

Garcia JJ (2008) Simulation of high tensile Poisson’s ratios of articular cartilage with a finite element fibril-reinforced hyperelastic model. Med Eng Phys 30: 590–598.

Grellmann WA, Berghaus EJ, Haberland Y, et al. (2006) Determination of strength and deformation behavior of human cartilage for the definition of significant parameters. J Biomed Mater Res A 78: 168–174.

Harris T (2010) How CAT scans work. Retrieved from http://health.howstuffworks.com/cat-scan.htm

Ilchenko GV, Ishchenko OYu, Lynova EN, Prishchep LV (2018) Assessment of organizational loyalty in medical institutions. International Journal of Medicine and Psychology 1(4): 24 – 36.

Kim DW, Gurney T (2006) Management of naso-septal L-strut deformities. Facial Plast Surg 22: 9-27.

Lee et al. (2010) Biomechanics of the Deformity of Septal L-Struts. Laryngoscope 120: August: 1508.

Mau T, Mau ST, Kim DW (2007) Cadaveric and engineering analysis of the septal L-strut. Laryngoscope 117: 1902–1906.

Mowlavi A, Masouem Kalkanis J, Guyuron B (2006) Septal cartilage defined: implications for nasal dynamics and rhinoplasty. Plast Reconstr Surg 117: 2171–2174.

Naumann A, Dennis JE, Awadallah A, et al. (2002) Immunochemical and mechanical characteristics of cartilage subtypes in rabbit. J Histochem Cytochem 50: 1049–1058.

Pena E, Calvo B, Martinez MA, Doblare M (2006) A three-dimensional finite element analysis of the combined behavior of ligaments and menisci in the healthy human knee joint. J Biomech 39: 1686–1701.

Richmon JD, Sage A, Van Wong W, Chen AC, Sah RL, Watson D (2006) Compressive biomechanical properties of human nasal septal cartilage. Am J Rhinol 20: 496–501.

Richmon JD, Sage AB, Wong VW, et al. (2005) Tensile biomechanical properties of human nasal septal cartilage. Am J Rhinol 19: 617–622.

Salalykina EV, Papikyan OA (2018) Issues of optimization of work of nursing personnel under conditions of the central district hospital. International Journal of Medicine and Psychology 1(2): 12 – 16.

Vicente GS, Buchart C, Borro D, Celigueta JT (2008) Maxillofacial surgery simulation using a mass-spring model derived from continuum and the scaled displacement method. Int J Comput Assist Radiol Surg 4: 89–98.

Westreich RW, Courtland HW, Nasser P, Jepsen K, Lawson W (2007) Defining nasal cartilage elasticity: biomechanical testing of the tripod theory based on a cantilevered model. Arch Facial Plast Surg 9: 264–270.

Westreich RW, Lawson MW (2008) The tripod theory of nasal tip support revisited: the cantilevered spring model. Arch Facial Plast Surg 10: 170–179.

Wilson W, van Donkelaar CC, van Rietbergen R, Huiskes R (2005) The role of computational models in the search for the mechanical behavior and damage mechanisms of articular cartilage. Med Eng Phys 27: 810–826.